

The production of charged-kaon pairs in proton-antiproton collisions: The role of higher-twist mechanism

M. Demirci^{1,*} and A. I. Ahmadov^{2,†}

¹*Department of Physics, Karadeniz Technical University, TR61080 Trabzon, Turkey*

²*Department of Theoretical Physics, Baku State University, AZ1148 Baku, Azerbaijan*

(Dated: October 4, 2018)

The higher-twist (HT) contribution to the charged kaon pair production in the high energy proton-antiproton collisions at large transverse momentum p_T is investigated by using the frozen coupling constant approach for various kaon distribution amplitudes (DAs), which are predicted by light-cone formalism, the light-front quark model, the nonlocal chiral quark model and the light-front holographic AdS/CFT approach. In the numerics the dependencies of the HT contribution on the transverse momentum p_T , the rapidity y , and the variable x_T are discussed with special emphasis put on DAs. The HT contribution is also compared with the leading-twist ones. It is shown that the HT contributions are dependent on the kaon DAs and also some other phenomenological parameters such as momentum cut-off parameter Δp . Inclusive kaon pair production presents a remarkable test case in which HT terms dominate those of LT in certain kinematic regions. The HT direct production process via gluon-gluon fusion contributes significantly to the inclusive cross section at large p_T .

PACS numbers: 12.38.Bx, 13.60.Le, 13.85.Dz, 13.87.Fh

I. INTRODUCTION

The hadron production has been investigated for a long period in high-energy physics and nuclear physics, as well as cosmic-ray physics. The absolute yields and the transverse momentum (p_T) spectra of identified hadrons are among the fundamental physical observables in high-energy hadron-hadron collisions. These observables could be used to check and refine phenomenological models of the strong interaction. Furthermore, the search for large- p_T hadron-hadron productions has contributed essentially to our understanding of the nature of short-distance parton-parton interactions. Particularly with the advent of the high-energy proton-antiproton collisions, such interactions have been successfully explained by using the well-known techniques of perturbation theory.

In the standard perturbative Quantum Chromodynamics (pQCD) picture, hadrons are produced by the parton jet fragmentation. However, higher-twist (HT) processes can also be used as production mechanism. The term “twist” emerged in the operator product expansion (OPE), which was a method used for obtaining predictions of pQCD in deep inelastic scattering [1]. Today, the term refers to contributions suppressed by powers of large momentum with respect to the leading terms. The leading-twist (LT) is standard processes of the pQCD within the collinear factorization, where hadrons are produced through fragmentation processes. On the other hand, HT processes are taken usually as direct hadron production, in which the hadron is produced directly in

the hard subprocess rather than by quark/gluon fragmentation [2].

In the last forty years, HT effects in QCD have been investigated by many researchers for various phenomena (see, e.g., Refs. [3–8]). The results of these studies show that, the HT contributions to the cross sections and other characteristics of different processes may be considerable in some regions of the phase space, and the HT contributions are strongly dependent on the choice of the hadronic wave functions, hence the distribution amplitudes (DAs). The hadronic DAs in view of internal structure degrees of freedoms are essential for obtaining accurate predictions in QCD. The HT processes have also importance in understanding of Baryon anomaly, appeared in measurements of large- p_T hadron production at RHIC [9]. More research is needed to clarify the nature of the HT effects in QCD. Meson pair production in a hadron collider at large- p_T can be used as a short distance probe of the incident hadrons.

In the present work, we examine the HT effect on charged-kaon pair production at proton-antiproton collisions for different kaon DAs predicted by pQCD evaluation, light-cone formalism, the light-front quark model, the nonlocal chiral quark model and the light-front holographic AdS/CFT correspondence. The physical information of the inclusive kaon pair production can be obtained efficiently in the pQCD and it is, hence, possible to compare directly with the experimental data. The corresponding hard-scattering subprocesses occur via three different mechanisms: Direct production (kaons are produced directly at the hard-scattering subprocess), semi-direct production (one kaon is produced from jet fragmentation, while the other one is directly produced) and double jet production and fragmentation (both kaons are produced from fragmentation of the final quarks or gluons). The first two mechanisms are of HT, while the last

* mehmetdemirci@ktu.edu.tr

† ahmadovazar@yahoo.com

one corresponds to LT contributions. Therefore, we must systematically compare these different mechanisms.

We use the frozen coupling constant (FCC) approach during numerical evaluation. Although the FCC approach was introduced a long time ago [10–12], it is still interesting in nowadays [13–16]. For first time, it has originated from the divergent infrared behavior of the renormalization group expression for α_s . The FCC can be used in the infrared domain since it is a constant. The other reason for using this approach is that the pQCD coupling is running, and the effects of running α_s should be taken into account in every calculation. On the other hand, this makes some QCD calculations very difficult. However, for approximate predictions, it may be convenient to use some effective coupling which imitates the running of α_s in the perturbative domain. To get an agreement with experimental data, the value of the FCC is generally set from purely phenomenological predictions. Furthermore, it is used in combination with other phenomenological parameters to define hadronic processes. The fixed α_s has been used in various calculations carried out in the framework of the leading logarithmic approximation where the most important logarithmic contributions are completely resummed whereas argument of α_s is set off a posteriori from physical predictions.

The another way is through solution of the Schwinger-Dyson equations (SDE) for investigating the infrared behavior of the running coupling constant, gluon (and ghost) propagator at low energies [17]. In order to get infrared finite propagators, one can use a method where the gluon acquires a dynamical mass m_g^2 (see, e.g., Ref. [18]), and the another is that the gluon propagator goes to zero when the momentum $Q^2 \rightarrow 0$ (discussed in Refs. [19, 20]). In both cases, there appear the freezing of coupling constant in the infrared domain. In the case where squared momentum of hard gluon gets the form $Q^2 \rightarrow Q^2 + m_g^2$, argument of running coupling constant takes also the same form. Here m_g is interpreted as an effective dynamical mass of gluon.

The experimental researches on measurements of charged hadrons (or charged tracks) in proton-antiproton collisions have been carried out at $\sqrt{s} = 0.630, 1.8, 1.96$ TeV by CDF [21–23] and $\sqrt{s} = 0.5, 0.9, 7$ TeV by UA (CMS) [24]. For different center of mass energies, the differential cross sections are constructed and compared to a scaling with the variable $x_T = 2p_T/\sqrt{s}$. We provide our calculations at $\sqrt{s} = 500$ GeV. To compared with other energies we also present distribution of the variable x_T for a given p_T .

Kaon pair production in photon-photon and proton-antiproton collisions have been studied from high to low energies during the last years, using different methods such as HT mechanism, central exclusive production mechanism, effective meson theory, and standard pQCD (see, [25–28] and references therein).

The present work is organized as follows. In the next section, we provide some expressions for the HT (in

Sec. II A) and LT (in Sec. II B) contributions to cross section of the process $p\bar{p} \rightarrow K^+K^-X$ and a brief review for kinematics variables and convolution of contributions (in Sec. II C). In Sec. III, we give some DAs of kaon used in our calculations and their evolutions according to the scale Q . In Sec. IV, we present numerical results and discuss the dependence of the cross sections on the kaon DAs and other physical parameters in detail. Finally, the summary and concluding remarks are given in Sec. V.

II. THE ANALYTICAL RESULTS OF KAON PAIR PRODUCTION

The almost scale-invariant behavior of two-particle (gluon and quark) hard-scattering processes is a fundamental property of asymptotic freedom and QCD. If these hard-scattering subprocesses are convoluted with the parton distribution functions (PDFs) of the initial hadrons and the fragmentation functions (FFs) which produce final state interactions, the resulting inclusive cross section scales as $1/p_T^n$.

In the present study, we aim to investigate the inclusive production of kaon pairs with large- p_T in $p\bar{p}$ collisions. For this, we consider HT contributions to the cross section by using the FCC approach for different kaon DAs. Furthermore, HT contributions are compared with LT ones. This comparison will allow us to determine such regions in the phase space where HT contributions are essentially observable. In order to obtain an accurate value of the ratio contributions of HT and LT, we use the fact that prompt kaons are “non-accompanied” by any other hadron. However, this is not valid for the general case in which particles are occurring from the jets fragmentation. This criterion can be incorporated into the general formulas via a momentum cut-off parameter Δp [29].

We present details of analytical calculations on HT and LT contributions in the following subsections.

A. Higher-Twist Contributions

For HT contribution to the charged kaon pair production, there are two different mechanisms included in the hard scattering subprocess:

- i. Direct-production* (Fig. 1a): Both kaons are produced directly,
- ii. Semi-direct production* (Fig. 1b): One kaon is produced directly and the other one is produced from jet fragmentations.

The differential cross section for partonic subprocess is given by

$$\frac{d\hat{\sigma}(ab \rightarrow cd)}{d\cos\theta} = \frac{1}{32\pi\hat{s}} \sum |\overline{\mathcal{M}}|^2 \quad (2.1)$$

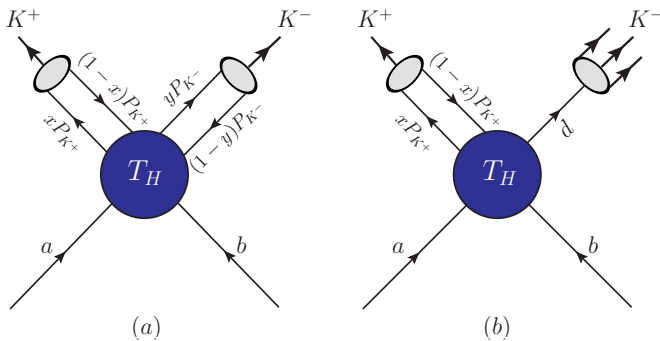


FIG. 1. Factorization of the kaon pair production amplitude in QCD at large momentum transfer in case of (a) direct production and (b) semi-direct production. The labels a, b, d represent quarks or gluons.

where \mathcal{M} is the invariant amplitude of the HT hard-scattering subprocesses and the bar on it refers to the average over initial spins and colours.

In order to obtain the corresponding amplitude \mathcal{M} , one should take integrations with the kaon DAs over the longitudinal momentum fractions x_i and y_i carried by the kaons's quark and antiquark. In light of this discussion, it takes the following form [30]:

$$\mathcal{M}(\hat{s}, \theta) = \int_0^1 [dx_i] \int_0^1 [dy_i] \Phi_{K^-}(y_i, \tilde{Q}_y) \times T_H(x_i, y_i; \hat{s}, \theta) \Phi_{K^+}(x_i, \tilde{Q}_x) \quad (2.2)$$

where $[dx_i] = \delta(1 - \sum_{k=1}^n x_k) \prod_{k=1}^n dx_k$ and n is the number of the valance quarks. The scale \tilde{Q} can be taken as $\tilde{Q}_x = \min(x, 1-x)Q$ and similarly $\tilde{Q}_y = \min(y, 1-y)Q$. T_H is the hard-scattering amplitude of subprocess for the production of the valance quarks collinear with each kaon. $\Phi(x, \tilde{Q}_x)$ is the quark distribution amplitude of the kaon (see Sec. III for details), sharing fractions x and $(1-x)$ of the kaon's total momentum. Similarly, $\Phi(y, \tilde{Q}_y)$ is sharing fractions y and $(1-y)$ of the other kaon's total

momentum. They were integrated over transverse momenta $k_T < Q$.

In pQCD calculations, the amplitude T_H at the leading order strongly depends on the renormalization scale, but does not depend on the factorization scale. However, one-loop QCD corrections to T_H lead to its explicit dependence on the both scales. Moreover, it should be noted that both scales can be chosen autonomously since they are independent of each other. In principle, under any choice of renormalization scheme and scale, all measurable quantities in QCD must be invariant. The use of different schemes and scales can lead to different theoretical predictions. Therefore, the constructive mathematical apparatus for defining QCD is a choice of the renormalization scale which makes scheme independent results at all fixed order in running coupling constant α_s .

Let us now give more details on the hard-scattering subprocesses for direct and semi-direct productions of the charged K-meson pair. To make the analysis of collinear divergences easier, we assume that both kaons are emitted at $\cos(\theta) = 0$ (θ is the emission angle measured in the center-of-mass frame), with equal p_T . We neglect all quark and kaon masses in all diagrams contributing to the hard-scattering subprocess at leading order, resulting in errors only of order $m^2/s \ll 1$.

i. For direct kaon pair production, we take the following hard-scattering subprocesses:

$$\begin{aligned} \diamond & gg \rightarrow K^+ K^-, \\ \diamond & q\bar{q} \rightarrow K^+ K^- \text{ for } q = u \text{ and } s. \end{aligned}$$

We show some Feynman diagrams for these subprocesses in Fig. 2. At each vertex (where three lines join) the interaction is proportional to the QCD coupling constant α_s , so if the cross section of the direct-production process is computed, it would be ended up with a number proportional to the 4 power of α_s . For direct kaon pair production, after averaging over colors and spins of incoming particles, the associated differential cross sections are written via the electromagnetic form factor of the kaon F_K as follows:

$$\frac{d\hat{\sigma}(gg \rightarrow K^+ K^-)}{d \cos \theta} = \frac{\pi \alpha_s^2 F_K^2}{18 \hat{s}} \left[\frac{1}{I_K} \int_0^1 dx \int_0^1 dy \frac{\Phi_K(x, \tilde{Q}_x) \Phi_K(y, \tilde{Q}_y)}{x(1-x)y(1-y)} \frac{x(1-x) + y(1-y)}{xy + (1-x)(1-y)} \right]^2, \quad (2.3)$$

$$\frac{d\hat{\sigma}(q\bar{q} \rightarrow K^+ K^-)}{d \cos \theta} = \frac{\pi \alpha_s^2 F_K^2}{972 \hat{s}} \left[\frac{1}{I_K} \int_0^1 dx \int_0^1 dy \frac{\Phi_K(x, \tilde{Q}_x) \Phi_K(y, \tilde{Q}_y)}{x(1-x)y(1-y)} \left(7 - 16xy - \frac{2x(1-2y(x+y)) - 4x^2 + 4xy}{xy + (1-x)(1-y)} \right) \right]^2. \quad (2.4)$$

where F_K and I_K are given by

$$F_K(\hat{s}) = \frac{16\pi\alpha_s}{3\hat{s}} \frac{f_K^2}{12} I_K^2, \quad (2.5)$$

$$I_K = \int_0^1 \frac{\Phi_K(x, \tilde{Q}_x)}{x(1-x)} dx. \quad (2.6)$$

The leading order hard scattering amplitudes exhibit divergence at both end points of x and y . However, the

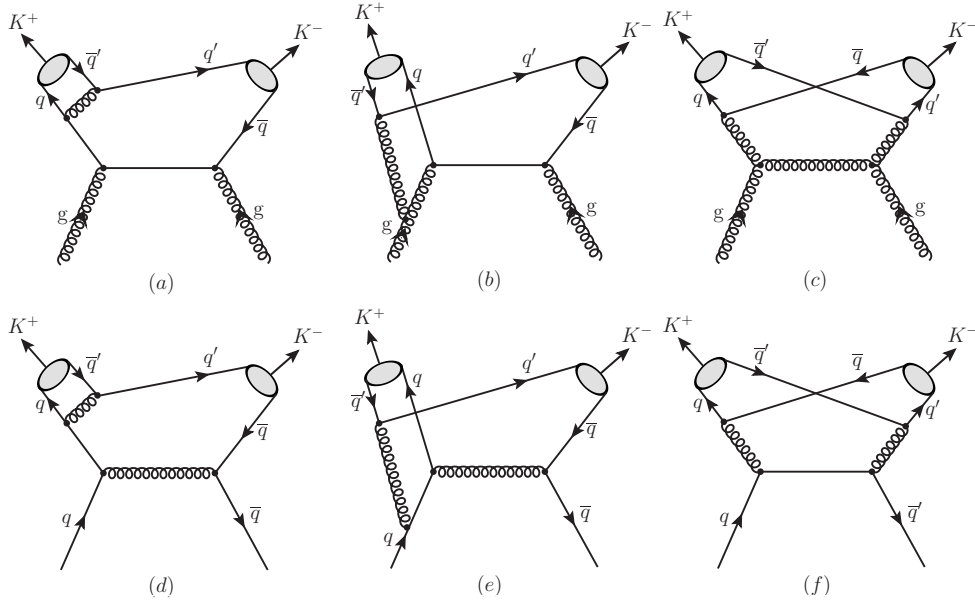


FIG. 2. QCD Feynman diagrams of the subprocesses $gg \rightarrow K^+ K^-$ and $q\bar{q} \rightarrow K^+ K^-$ for direct kaon pair production at leading order. The gray ovals indicate to the wave functions of kaons.

end point singularities are suppressed by the bound state quark DAs.

ii. There are two types of subprocesses for the semi-direct production:

- ◇ $q\bar{q}' \rightarrow K^\pm g$ where the gluon is fragmented to Kaon ($g \Rightarrow K^\mp$),
- ◇ $qg \rightarrow K^\pm q'$ (and $\bar{q}g \rightarrow K^\pm \bar{q}'$) where the final quark is fragmented to Kaon ($(\bar{q}') \Rightarrow K^\mp$).

In Fig. 3, we show some Feynman diagrams for subprocesses of semi-direct production. We note that there are

crossing symmetry among the invariant amplitudes associated with the subprocesses $q\bar{q}' \rightarrow K^\pm g$ and $qg \rightarrow K^\pm q'$, which can be directly checked by crossing exchanges $\hat{s} \leftrightarrow -\hat{t}$ at fixed \hat{u} in the invariant amplitude squared (summed over spin and color indices). At each vertex the interaction is proportional to the coupling constant α_s , so the cross section of semi-direct production process would be end up with a number proportional to the 3 power of α_s as seen in Fig. 3. Summing overall diagrams of either type, the corresponding differential cross sections of semi-direct production for each subprocess are given by

$$\frac{d\hat{\sigma}(q\bar{q}' \rightarrow K^\pm g)}{d\cos\theta} = \frac{32\pi\alpha_s^2}{81\hat{s}} \frac{16\pi\alpha_s}{3\hat{s}} \frac{f_K^2}{12} \left[\int_0^1 dx \frac{\Phi_K(x, \tilde{Q}_x)}{x(1-x)} \right]^2, \quad (2.7)$$

$$\frac{d\hat{\sigma}(qg \rightarrow K^\pm q')}{d\cos\theta} = \frac{5\pi\alpha_s^2}{108\hat{s}} \frac{16\pi\alpha_s}{3\hat{s}} \frac{f_K^2}{12} \left[\int_0^1 dx \frac{\Phi_K(x, \tilde{Q}_x)}{x(1-x)} \right]^2, \quad (2.8)$$

$$\frac{d\hat{\sigma}(\bar{q}g \rightarrow K^\pm \bar{q}')}{d\cos\theta} = \frac{5\pi\alpha_s^2}{108\hat{s}} \frac{16\pi\alpha_s}{3\hat{s}} \frac{f_K^2}{12} \left[\int_0^1 dx \frac{\Phi_K(x, \tilde{Q}_x)}{x(1-x)} \right]^2. \quad (2.9)$$

The initial q, \bar{q} and g are the constituent of the initial target proton and anti-proton, respectively.

B. Leading-Twist Contributions

It is also essential to examine effects of the HT contributions as well as to compare of HT contributions with LT ones for problems of the pQCD. From this comparison

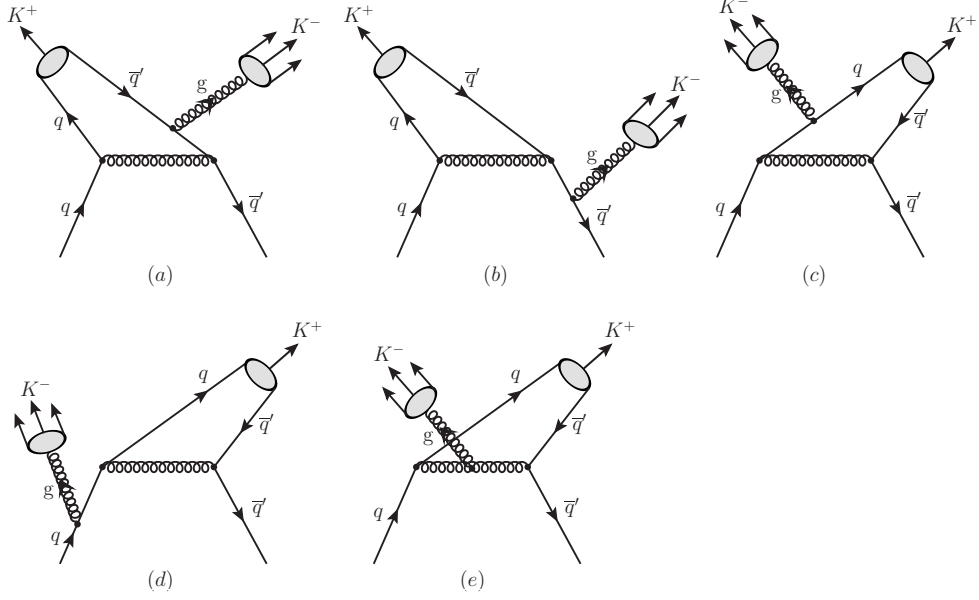


FIG. 3. QCD Feynman diagrams of the subprocess $q\bar{q}' \rightarrow K^+g$ (where the gluon is fragmented to kaon K^-) for semi-direct kaon pair production at leading level. The gray ovals indicate to the corresponding wave functions. Additionally, the diagrams corresponding to the subprocess $qg \rightarrow K^+q'$ (where the quark q' is fragmented to kaon K^-) can be plotted by exchanging the outgoing gluon and the incoming antiquark lines (which become a quark line) in each of above diagrams.

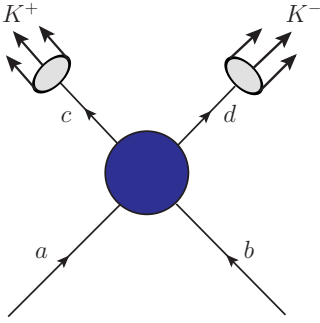


FIG. 4. A general diagram for the leading-twist subprocesses $ab \rightarrow cd$ where the final partons are fragmented into the charged kaon pairs, separately.

we can determine such regions in the phase space where HT contributions are actually observable. For LT contributions to the charged K -meson pair production in $p\bar{p}$ collisions, we consider the following hard subprocesses:

- ◇ $q\bar{q} \rightarrow q\bar{q} : q \Rightarrow K^+, \bar{q} \Rightarrow K^-$,
- ◇ $q\bar{q} \rightarrow q'\bar{q}' : q' \Rightarrow K^+, \bar{q}' \Rightarrow K^-$,
- ◇ $q\bar{q}' \rightarrow q\bar{q}' : q \Rightarrow K^+, \bar{q}' \Rightarrow K^-$,
- ◇ $q\bar{q} \rightarrow gg : g \Rightarrow K^+, g \Rightarrow K^-$,
- ◇ $qg \rightarrow qg : q \Rightarrow K^+, g \Rightarrow K^-$,

- ◇ $gg \rightarrow gg : g \Rightarrow K^+, g \Rightarrow K^-$ and
- ◇ $gg \rightarrow q\bar{q} : q \Rightarrow K^+, \bar{q} \Rightarrow K^-$,

where the symbol “ \Rightarrow ” represents fragmentation. We plot a representative diagram for these subprocesses in Fig. 4. In Table I, we list the associated expressions for differential cross sections of the LT subprocesses given in [1]. The initial and final state colors and spins have been averaged and summed, respectively. The cross sections for these QCD-hard subprocesses are dominated by \hat{t} -channel gluon exchange contributions. If the kaons are

TABLE I. The associated differential cross sections for the leading-twist subprocesses. The primed symbol (q') denotes distinct flavor and $\hat{s}, \hat{t}, \hat{u}$ are the Mandelstam variables of the subprocess.

$ab \rightarrow cd$	$\frac{d\hat{\sigma}(ab \rightarrow cd)}{d \cos \theta}$
$q\bar{q} \rightarrow q\bar{q}$	$\frac{\pi\alpha_s^2}{2\hat{s}} \frac{4}{9} \left(\frac{\hat{u}^2 + \hat{s}^2}{\hat{t}^2} + \frac{\hat{u}^2 + \hat{t}^2}{\hat{s}^2} - \frac{2}{3} \frac{\hat{u}^2}{\hat{s}\hat{t}} \right)$
$q\bar{q} \rightarrow q'\bar{q}'$	$\frac{2\pi\alpha_s^2}{9\hat{s}} \left(\frac{\hat{u}^2 + \hat{t}^2}{\hat{s}^2} \right)$
$q\bar{q}' \rightarrow q\bar{q}'$	$\frac{2\pi\alpha_s^2}{9\hat{s}} \left(\frac{\hat{u}^2 + \hat{s}^2}{\hat{t}^2} \right)$
$q\bar{q} \rightarrow gg$	$\frac{\pi\alpha_s^2}{2\hat{s}} \frac{8}{3} \left(\frac{4}{9} \frac{\hat{u}^2 + \hat{t}^2}{\hat{u}\hat{t}} - \frac{\hat{u}^2 + \hat{t}^2}{\hat{s}^2} \right)$
$qg \rightarrow qg$	$\frac{\pi\alpha_s^2}{2\hat{s}} \left(\frac{\hat{u}^2 + \hat{s}^2}{\hat{t}^2} - \frac{4}{9} \frac{\hat{u}^2 + \hat{s}^2}{\hat{u}\hat{s}} \right)$
$gg \rightarrow gg$	$\frac{\pi\alpha_s^2}{\hat{s}} \frac{9}{4} \left(3 - \frac{\hat{u}\hat{t}}{\hat{s}^2} - \frac{\hat{u}\hat{s}}{\hat{t}^2} - \frac{\hat{s}\hat{t}}{\hat{u}^2} \right)$
$gg \rightarrow q\bar{q}$	$\frac{\pi\alpha_s^2}{2\hat{s}} \left(\frac{1}{6} \frac{\hat{u}^2 + \hat{t}^2}{\hat{u}\hat{t}} - \frac{3}{8} \frac{\hat{u}^2 + \hat{t}^2}{\hat{s}^2} \right)$

produced at emission angle $\theta = 90^\circ$ with the rapidities of

final particles $y_1 = y_2 = 0$, the hard scattering cross section $d\sigma/d\hat{t}$ is actually probed at angles around $\theta = 90^\circ$, hence $\hat{t} = \hat{u} = -\hat{s}/2$.

The LT contributions to production of kaon pairs at large p_T in proton-antiproton collisions are conventionally analyzed within the framework of pQCD by convoluting the hard subprocess cross sections given in Table I with evolved FFs and PDFs.

C. The Convolution of Twist Contributions in Proton-Antiproton Collisions

Let us now consider the hadronic process of the charged K-meson pair production

$$p\bar{p} \rightarrow K^+K^- + X \quad (2.10)$$

where X indicates all other particles in the final state. We assume that both kaons in the $p\bar{p}$ collisions are emitted at 90° in the center-of-mass frame, with equal p_T . We apply the factorization formula predicted by Gunion and Petersson [31]. In this approach, in order to obtain inclusive production of the charged-kaon pair (2.10), differential cross section of the corresponding hard-scattering subprocess¹ is convoluted with the two PDFs and two FFs:

$$\begin{aligned} \Sigma_{K^+K^-} \equiv \frac{EE'd\sigma(p\bar{p} \rightarrow K^+K^-X)}{d^3pd^3p'} &= \frac{1}{(\pi\sqrt{s})^2 < k_T^2 >} \int_{z_{min}}^1 \frac{dz}{z^2} \int_{z_{min}}^1 \frac{dz'}{z'^2} F(z, z') G_{a/p_1}(x_1, \mu_F^2) G_{b/p_2}(x_2, \mu_F^2) \\ &\times \frac{d\hat{\sigma}(ab \rightarrow cd)}{d\cos\theta} D_c^{K^+}(z, Q^2) D_d^{K^-}(z', Q^2), \end{aligned} \quad (2.11)$$

where \sqrt{s} is the center-of-mass energy of main process, $< k_T^2 >$ is the mean square of the intrinsic partonic momentum for partons a, b . The functions G_{a/p_1} and G_{b/p_2} are the universal PDFs for the partons a, b in the proton and antiproton p_1, p_2 , respectively. They depend on the longitudinal momentum fractions of the two partons in case final jets fragmenting into kaon pairs, $x_1 = x_2 \cong 2p_T/\sqrt{zz's}$. Dynamical properties of the jets are close to the parton carried a fraction of momentum of parent hadron. The correlation function $F(z, z')$ is denoted by

$$F(z, z') = \frac{z + z'}{2\sqrt{zz'}} \exp \left[\frac{-(z - z')^2 p_T^2}{2z^2 z'^2 < k_T^2 >} \right]. \quad (2.12)$$

In our numerical evaluations, the functions $D_c^{K^+}(z, Q^2)$ and $D_d^{K^-}(z', Q^2)$ in Eq. (2.11) are taken for each different production mechanism as follows:

- $D_{K^+}^{K^+}(z, Q^2) = \delta(1-z)$ and $D_{K^-}^{K^-}(z', Q^2) = \delta(1-z')$ in case of direct kaon pair production ($c \equiv K^+$ and $d \equiv K^-$),
- $D_{K^+}^{K^+}(z, Q^2) = \delta(1-z)$, whereas $D_d^{K^-}(z', Q^2)$ is the usual FF in case of semi-direct kaon pair production ($c \equiv K^+$ and $d \equiv \bar{u}, s, g$),
- $D_c^{K^+}(z, Q^2)$ and $D_d^{K^-}(z', Q^2)$ are the usual FFs for leading-twist contributions,

where $D_{c,d}^K$ indicates the quark fragmentation function into a kaon including a quark of the same flavor. For leading-twist subprocesses, the kaons are indirectly emitted from the final partons with fractional momenta z, z' . In the numerical treatment, we use the usual FFs in [32], parameterized as

$$D_{c,d}^h(z, Q^2) = N z^\alpha (1-z)^\beta (1+z)^\gamma. \quad (2.13)$$

Furthermore, we use the MSTW2008 PDFs[33] for the quark and gluon distribution functions inside the proton and antiproton.

The minimum value of the momentum fraction of the final parton is defined in this form:

$$z_{min} = \frac{p_T}{p_T + \Delta p} \quad (2.14)$$

where momentum cut-off parameter Δp defines the experimental upper limit for non-detection of one or more particles accompanying either kaon detected. When this limit is exceeded, the corresponding event will be refused. The prompt kaons appear non-accompanied by any other hadron, but this is not the case, in general, for particles produced from jet fragmentation.

The longitudinal momentum fractions of partons are defined in the following forms

$$x_1 = \frac{p_T}{\sqrt{s}} (e^{y_1} + e^{y_2}), \quad (2.15)$$

$$x_2 = \frac{p_T}{\sqrt{s}} (e^{-y_1} + e^{-y_2}), \quad (2.16)$$

in which y_1, y_2 are the rapidities of the final particles. We use the kinematic expressions discussed in Ref. [1] and in our previous works [34–36].

¹ We indicate the higher-twist cross section by $\Sigma_{K^+K^-}^{HT}$ and the leading-twist cross section by $\Sigma_{K^+K^-}^{LT}$.

We note that the higher-twist cross sections are proportional to \hat{s}^{-4} for direct-production and \hat{s}^{-3} for semi-direct production, hence, they have the form of p_T^{-8} and p_T^{-6} , respectively. However, the p_T^{-6} processes $q\bar{q} \rightarrow Mq$ and $gq \rightarrow Mq$ are interesting in high- p_T meson production processes such as $pp \rightarrow MX$ because the meson is produced directly in the subprocess without the fragmentation. In fact the contributions of standard p_T^{-4} scaling processes such as $qq \rightarrow qq$, $gg \rightarrow gg$ and $gq \rightarrow gq$ are highly suppressed by 2 to 3 orders of magnitude relative to the "directly coupled" contributions because of the suppression of jet fragmentation $D_q^M(z)$ at large momentum fraction z and the fact that the subprocesses must arise at a remarkably larger momentum transfer than that of the triggered particle [37, 38].

III. KAON DISTRIBUTION AMPLITUDES AND THEIR EVOLUTIONS

The important aspect of the present study is to select of the distribution amplitudes. DAs are intrinsically nonperturbative; they include all effects of collinear singularities, meson bound-state dynamics, nonperturbative interactions and confinement. The DA $\Phi_K(x, \mu^2)$ is the amplitude for the kaon consisting of a $q\bar{q}'$ pair, with the q and \bar{q}' collinear and on shell relative to the scale μ . During the past few decades, there have been many theoretical efforts to calculate the kaon DA using different methods such as lattice calculation, the QCD sum rule [39–41], the chiral-quark model, and the light-front quark model. In this study we choose several DAs which show significant differences compared to each other as follows: the asymptotic DA derived in pQCD evaluation [42], kaon DAs with six non-trivial Gegenbauer coefficients a_1, a_2, a_3, a_4, a_5 , and a_6 derived by using the light-cone formalism (LCQM) [43], obtained from the Gaussian wave function with harmonic oscillator potential and power-law wave function (HOP and PL, respectively) [44], and predicted within the framework of the nonlocal chiral quark model from the instanton vacuum (χ QM) [45].

The asymptotic DA is given by

$$\Phi_{asy}^K(x) = \sqrt{3}f_K x(1-x), \quad (3.1)$$

where $f_K = 156.01$ MeV. The overall normalization is

$$\begin{aligned} \Phi_K(x, \mu_0^2) = & \Phi_{asy}^K(x) \left[1 + 3a_1(2x-1) + a_2 \left(\frac{15}{2}(2x-1)^2 - \frac{3}{2} \right) + a_3 \left(\frac{35}{2}(2x-1)^3 - \frac{15}{2}(2x-1) \right) \right. \\ & + a_4 \left(\frac{315}{8}(2x-1)^4 - \frac{105}{4}(2x-1)^2 + \frac{15}{8} \right) + a_5 \left(\frac{693}{8}(2x-1)^5 - \frac{315}{4}(2x-1)^3 + \frac{105}{8}(2x-1) \right) \\ & \left. + a_6 \frac{35}{16} \left(\frac{429}{5}(2x-1)^6 - 99(2x-1)^4 + 27(2x-1)^2 - 1 \right) \right] \end{aligned} \quad (3.5)$$

set by the kaon decay constant via

$$\int_0^1 \Phi_K(x, \mu^2) dx = \frac{f_K}{2\sqrt{3}}. \quad (3.2)$$

The evolution of the DA on the scale Q^2 is obtained by solving a Bethe-Salpeter type equation. The most general solution is an expansion in the Gegenbauer polynomials $C_n^{3/2}$ as follow [42, 46]:

$$\begin{aligned} \Phi_K(x, Q^2) = & \Phi_{asy}^K(x) \left[1 + \sum_{n=1}^{\infty} a_n(Q^2) \right. \\ & \left. \times C_n^{3/2}(2x-1) \right] \end{aligned} \quad (3.3)$$

where the Gegenbauer coefficients a_n (also called Gegenbauer moments) can be determined by means of Gegenbauer polynomials orthogonality condition

$$\int_{-1}^1 (1-\zeta^2) C_n^{3/2}(\zeta) C_{n'}^{3/2}(\zeta) d\zeta = \frac{\Gamma(n+3)\delta_{nn'}}{n!(n+3/2)}. \quad (3.4)$$

The Gegenbauer moments a_n are very useful in investigating of the DAs since they form the shape of the corresponding hadron wave function. It can be derived from theoretical models or extracted from the experiments. In principle, these moments show how much the DAs deviate from the asymptotic one.

In Table II, we list values of the Gegenbauer moments used in our study. The DAs are created by opening up to the first six term of Eq. (3.3) as seen in Eq. (3.5) and then using the values of Gegenbauer moments in the following table. Then, we label them as follows: $\Phi_K^{LCQM}(x, Q^2)$,

TABLE II. The Gegenbauer moments of the HT kaon DAs obtained from the different methods at the scale $\mu_0 \sim 1$ GeV.

Moments a_n	LCQM [43]	HOP [44]	PL [44]	χ QM [45]
a_1	0.08	-0.1501	-0.0218	-0.00474
a_2	0.00	-0.1474	-0.0385	-0.11797
a_3	0.03	0.0198	-0.0003	-0.00298
a_4	-0.06	-0.0162	-0.0090	-0.01314
a_5	-0.14	0.0137	0.0004	-0.00068
a_6	-0.03	-0.0004	-0.0030	-0.00282

$\Phi_K^{HOP}(x, Q^2)$, $\Phi_K^{PL}(x, Q^2)$, and $\Phi_K^{\chi QM}(x, Q^2)$. The kaon DA can be written by the Gegenbauer-polynomial expansion up to the sixth moment as follows:

We also use the following kaon DAs

$$\Phi^{HOL}(x) = \frac{4}{\sqrt{3}\pi} \sqrt{x(1-x)} \quad (3.6)$$

and

$$\Phi^{AdS/CFT}(x) = \frac{A_1 \kappa_1}{2\pi} \sqrt{x(1-x)} e^{\left(-\frac{m^2}{2\kappa_1^2 x(1-x)}\right)} \quad (3.7)$$

derived by light-front holographic AdS/CFT correspondence (suggested by Brodsky and Téramond) [47, 48]. We checked that all the DAs can be normalized by using Eq. (3.2). We will dwell on the dependence of cross sections upon the model structure of the above DAs.

We depict in Fig. 5 the normalized kaon DAs for each models, using the normalization condition in Eq. (3.2). This figure indicate how much the DAs deviate from the asymptotic one. The kaon DAs vanish at the endpoints ($x = 0$ and $x = 1$) for all cases as expected. The asymptotic DA is symmetric around $x = 0.5$.

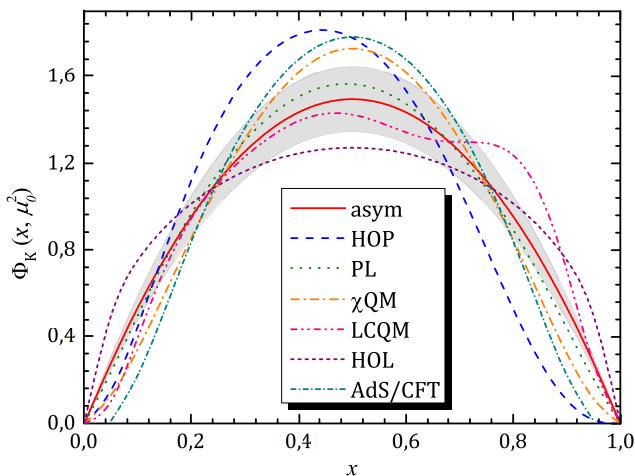


FIG. 5. Normalized DAs for kaon obtained from LCQM, HOP, PL, χ QM, HOL and AdS/CFT models compared with the asymptotic one (solid line). The gray band indicates $\pm 10\%$ of the asymptotic DA.

The evolution of the DA on the factorization scale Q^2 is governed by the functions $a_n(Q^2)$:

$$a_n(Q^2) = a_n(\mu_0^2) \left[\frac{\alpha_s(Q^2)}{\alpha_s(\mu_0^2)} \right]^{\gamma_n/\beta_0}, \quad (3.8)$$

where $\{\gamma_n\}$ are the one-loop anomalous dimensions defined by the expression,

$$\gamma_n = C_F \left[1 - \frac{2}{(n+1)(n+2)} + 4 \sum_{j=2}^{n+1} \frac{1}{j} \right], \quad (3.9)$$

and $\beta_0 = (11 - \frac{2}{3}n_f)$ is the one-loop coefficient of QCD beta function, n_f is the number of active flavors.

We note that at the boundary of $Q^2 = \mu_0^2$, Eq. (3.3) reduces to Eq. (3.5) with Gegenbauer moments given in

Table II, and in the limit $Q^2 \rightarrow \infty$, Eq. (3.3) evolves into the form of the asymptotic DA (3.1), as expected. However, with increasing Q^2 , the evolution of DA is very slow logarithmically and, at the present-day energies, DA might be different in form.

The QCD running coupling constant $\alpha_s(Q^2)$ at the one-loop approximation is given as

$$\alpha_s(Q^2) = \frac{4\pi}{(11 - \frac{2}{3}n_f) \ln(\frac{Q^2}{\Lambda^2})} \quad (3.10)$$

where Λ is the QCD scale parameter. The choice of renormalization scale in $\alpha_s(Q^2)$ is one of the main problems in QCD. In order to make the perturbation theory meaningful, the argument of the running coupling constant $\alpha_s(Q^2)$ should be fixed as the square of the momentum transfer of the exchanged gluon [49].

In the expression $\tilde{Q} = \min(x, 1-x)Q$, we freeze the variable x by taking its average value, namely, $\bar{x} = 1/2$. Additionally, the scale Q^2 can be taken as the average squared momentum transfer carried by the hard gluon in a given subprocess. Within FCC approach, we consider as follows:

$$\tilde{Q} = \begin{cases} \frac{p_T}{2}, & \text{for direct HT contribution} \\ \frac{1}{2} \frac{p_T}{\sqrt{z}}, & \text{for semi-direct HT contribution} \\ \frac{1}{2} \frac{p_T}{\sqrt{zz'}}, & \text{for LT contribution.} \end{cases}$$

IV. NUMERICAL RESULTS AND DISCUSSION

In this section, we discuss the numerical predictions for HT and LT contributions to cross section of the process $p\bar{p} \rightarrow K^+K^-X$ in detail. To have a quantitative understanding of the effects of HT contributions on the charged kaon pair production, it is convenient to compute the ratio of HT to LT contributions, namely, $\Sigma_{K^+K^-}^{HT}/\Sigma_{K^+K^-}^{LT}$. We have examined the dependence of HT and LT contributions to charged kaon pair production, their sum and their ratio on the transverse momentum p_T , the rapidity y of kaon pairs, and the variable x_T for seven different DAs predicted by light-cone formalism, the light-front quark model, the nonlocal chiral quark model and the light-front holographic AdS/CFT approach.

We plot the dependence of the HT, LT contributions, ratio of HT to LT and sum of HT and LT on the transverse momentum p_T ranging from 2 to 10 GeV/c at the center-of-mass energy $\sqrt{s} = 500$ GeV with rapidities of kaons $y = y_1 = y_2 = 0$ for momentum cut-off parameter $\Delta p = 0.5$ GeV/c in Fig. 6 and $\Delta p = 1$ GeV/c in Fig. 7. We do not compute HT and LT contributions for $p_T < 2$ GeV/c, however, since the theory of perturbation becomes increasingly less reliable in that region. Both LT and HT cross sections decrease smoothly with increasing the transverse momentum for each DAs. It is clear that HT contributions depend on the choice of different kaon DAs. Note that the DAs of LCQM, HOP, PL, and χ QM give results which are close in shape to those for the asymptotic DA, but $\Sigma_{K^+K^-}^{HOL}$ is larger and $\Sigma_{K^+K^-}^{AdS/CFT}$

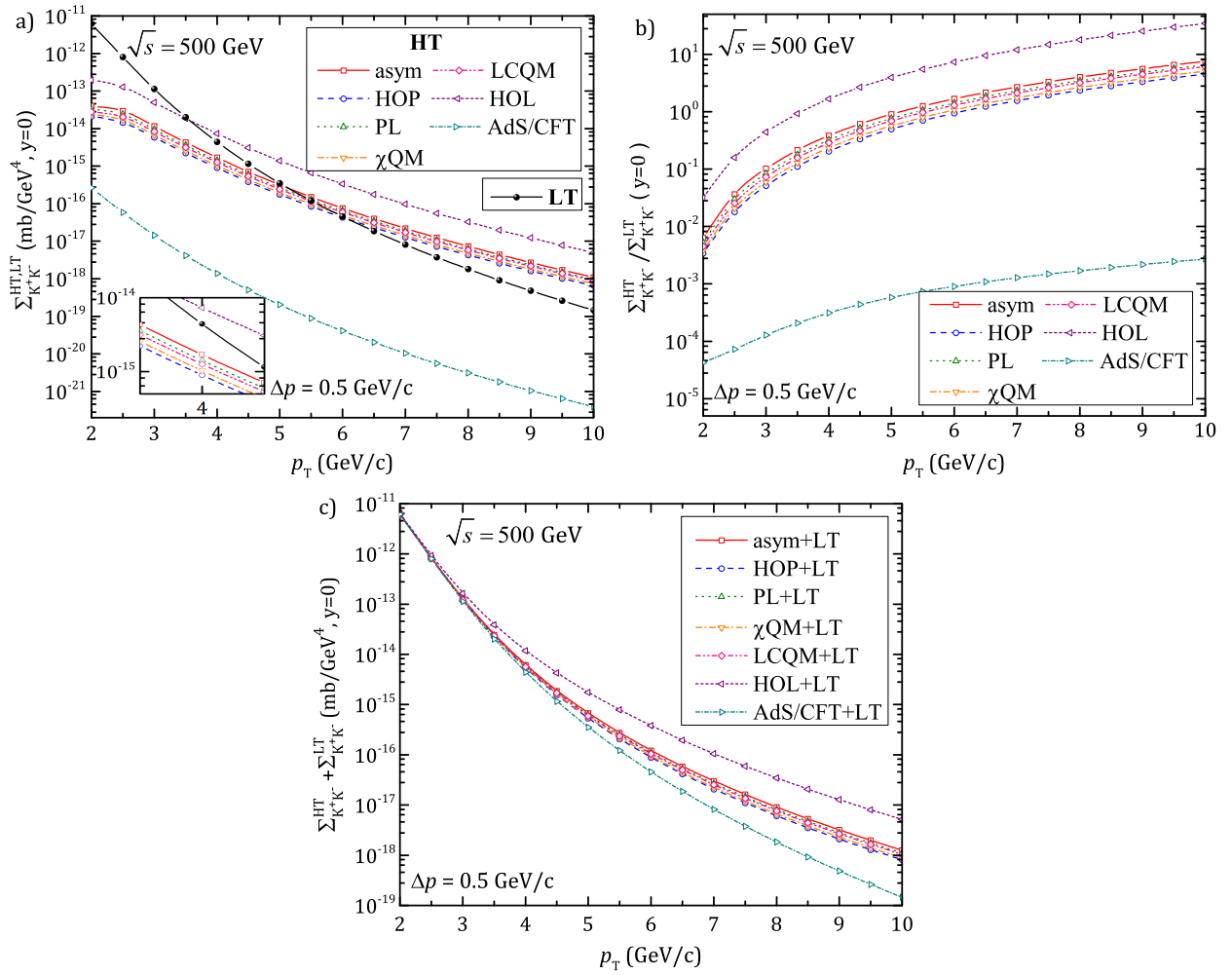


FIG. 6. a) LT and HT contributions to charged-kaon pair production $p\bar{p} \rightarrow K^+K^-X$, b) ratio of HT to LT and c) sum of these contributions as a function of the transverse momentum p_T for momentum cut-off parameter $\Delta p = 0.5$ GeV/c at $\sqrt{s} = 500$ GeV. The insert figure in (a) shows HT and LT contributions for a interval of p_T from 3.5 to 4.5 GeV/c.

is smaller than them by one and three orders of magnitude, respectively. The HT contribution calculated for HOL is roughly %77, %81, %82, %85, %87 and four order of magnitude larger than those for asym, PL, LQCM, χ QM, HOP and AdS/CFT, respectively. In other words, the HT contributions are sorted in descending order according to our DAs as $\Sigma_{K^+K^-}^{HOL} > \Sigma_{K^+K^-}^{asym} > \Sigma_{K^+K^-}^{PL} > \Sigma_{K^+K^-}^{LQCM} > \Sigma_{K^+K^-}^{\chi QM} > \Sigma_{K^+K^-}^{HOP} > \Sigma_{K^+K^-}^{AdS/CFT}$. In particular, the HT cross section in HOL, $\Sigma_{K^+K^-}^{HOL}$, reaches a value of 1.4×10^{-15} mb/GeV⁴ for both values of Δp at $p_T = 5$ GeV/c, while value of LT is 3.5×10^{-16} mb/GeV⁴ for $\Delta p = 0.5$ GeV/c and 1.4×10^{-14} mb/GeV⁴ for $\Delta p = 1$ GeV/c.

The ratio of HT to LT contributions will allow us to determine such regions in the phase space where HT contributions are essentially observable. The ratio, $\Sigma_{K^+K^-}^{HT}/\Sigma_{K^+K^-}^{LT}$, increases systemically with increasing the transverse momentum, because z_{min} comes closer to

1 and thus $\Sigma_{K^+K^-}^{LT}$ decreases. Figure 6(b) shows that $\Sigma_{K^+K^-}^{HT}/\Sigma_{K^+K^-}^{LT}$ at $\Delta p = 0.5$ GeV/c increases from 0.006 to 7.57 for asymptotic, 0.003 to 4.55 for HOP, 0.005 to 6.56 for the PL, 0.004 to 5.09 for χ QM, 0.004 to 6.12 for the LQCM, 0.032 to 34.54 for HOL and 4×10^{-5} to 0.003 for AdS/CFT when p_T runs from 2 to 10 GeV/c. Particularly, HT contributions become significant at $p_T \geq 5.5$ GeV/c for asym, HOP, PL, χ QM and LQCM, and $p_T \geq 3.5$ GeV/c for HOL. Figure 7(b) displays that $\Sigma_{K^+K^-}^{HT}/\Sigma_{K^+K^-}^{LT}$ at $\Delta p = 1$ GeV/c increases from 5×10^{-4} to 0.17 for asymptotic, 3×10^{-4} to 0.10 for HOP, 4×10^{-4} to 0.15 for the PL, 3×10^{-4} to 0.12 for χ QM, 4×10^{-4} to 0.14 for the LQCM, 0.002 to 0.74 for HOL and 5×10^{-6} to 2×10^{-4} for AdS/CFT when p_T runs from 2 to 10 GeV/c.

These results show that the ratio $\Sigma_{K^+K^-}^{HT}/\Sigma_{K^+K^-}^{LT}$ is mostly sensitive according to variation of the Δp and p_T . For small value of Δp , it reaches considerably larger values. The corresponding ratio, on the

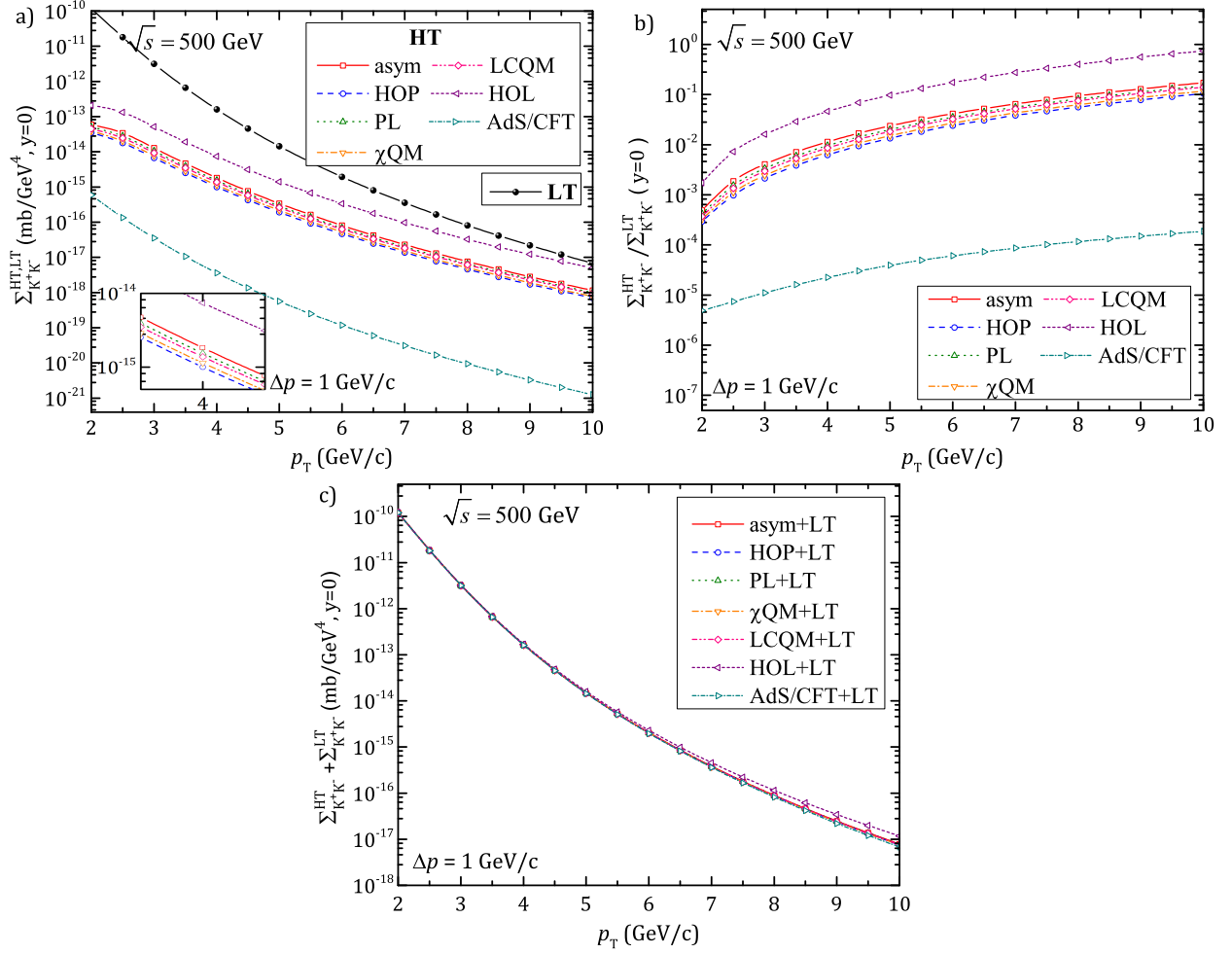


FIG. 7. The same as in Fig. 6, but for $\Delta p = 1$ GeV/c.

TABLE III. The individual HT contributions from direct and semi-direct hard-scattering processes at $p_T = 5$ GeV/c for each DAs, where all contributions are given in mb/GeV^4 .

DAs	Direct production		Semi-direct production		Ratio of HT to LT $\Sigma_{K^+K^-}^{\text{HT}}/\Sigma_{K^+K^-}^{\text{LT}}$
	$gg \rightarrow K^+K^-$	$q\bar{q} \rightarrow K^+K^-$	$q\bar{q}' \rightarrow K^\pm g$	$qg \rightarrow K^\pm q' + \bar{q}g \rightarrow K^\pm \bar{q}'$	
asym	3.06×10^{-15}	7.64×10^{-19}	3.46×10^{-19}	1.20×10^{-17}	0.907
HOP	1.65×10^{-16}	3.44×10^{-19}	2.70×10^{-19}	9.36×10^{-18}	0.498
PL	2.57×10^{-16}	5.91×10^{-19}	3.22×10^{-19}	1.12×10^{-17}	0.764
χQM	1.89×10^{-16}	3.45×10^{-19}	2.83×10^{-19}	9.83×10^{-18}	0.567
LCQM	2.32×10^{-16}	3.86×10^{-19}	3.10×10^{-19}	1.07×10^{-17}	0.691
HOL	1.29×10^{-15}	7.02×10^{-17}	6.16×10^{-19}	2.14×10^{-17}	4.096
AdS/CFT	1.74×10^{-21}	2.25×10^{-24}	5.65×10^{-21}	1.96×10^{-19}	0.001

other hand, increases by about two orders of magnitude for $\Delta p = 1$ GeV/c and three orders of magnitude for $\Delta p = 0.5$ GeV/c when the transverse momentum p_T varies from 2 to 10 GeV/c for each DA. The ratio of HT contributions calculated with $\Delta p = 0.5$ GeV/c and $\Delta p = 1$ GeV/c, are constant within around %93 for asym, HOP, χQM , LCQM, %99 for HOL and %35 for AdS/CFT between $p_T = 3$ and 10 GeV/c. The

LT cross section calculated with $\Delta p = 1$ GeV/c are, however, around %97 larger than one calculated with $\Delta p = 0.5$ GeV/c.

It is interesting to see what the relative contributions are of the different internal mechanisms. In Fig. 8, we present the dependence of the HT contributions from direct and semi-direct production, separately, on the transverse momentum p_T at $\sqrt{s} = 500$ GeV for each DA.

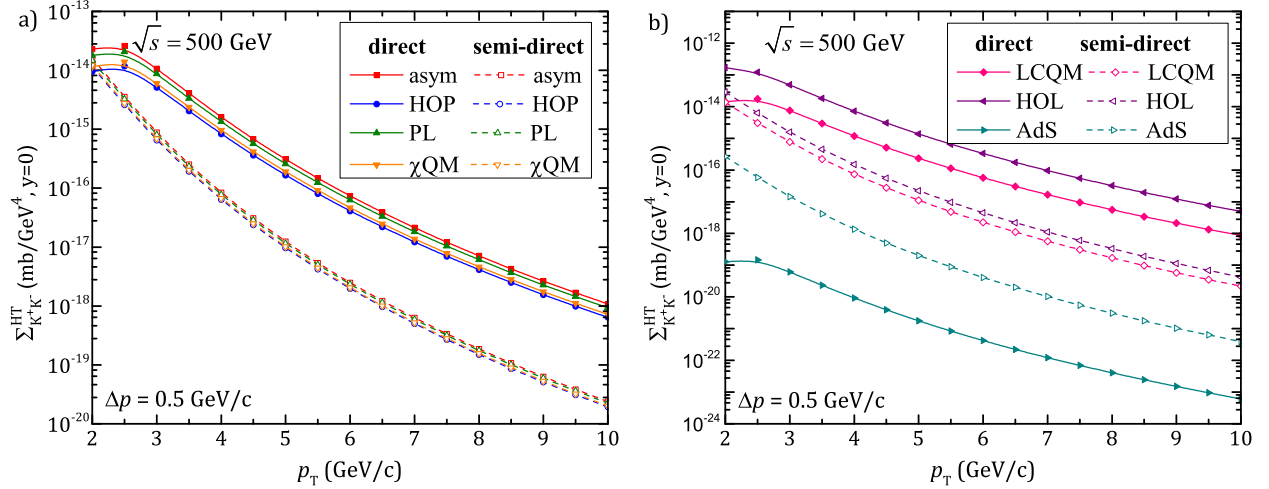


FIG. 8. a) HT contributions from direct and semi-direct production for a) asym, HOP, PL, and χ QM, b) LCQM, HOL and AdS/CFT as a function of the transverse momentum p_T for momentum cut-off parameter $\Delta p = 0.5$ GeV/c at $\sqrt{s} = 500$ GeV. The solid lines and dashed-lines indicate to HT contributions from direct-production and semi-direct production, respectively.

For direct kaon pair production, hard-scattering subprocesses are $gg \rightarrow K^+K^-$ and $q\bar{q} \rightarrow K^+K^-$ for $q = u$ and s . For semi-direct kaon pair production, hard-scattering subprocesses are $q\bar{q}' \rightarrow K^\pm g$ and $qg \rightarrow K^\pm q'$ (and $\bar{q}g \rightarrow K^\pm \bar{q}'$). Direct production processes make dominant contributions for asym, HOP, PL, χ QM, LCQM and HOL, while for AdS/CFT, semi-direct production processes have dominant contribution. When p_T runs from 2 to 10 GeV/c, HT contributions from direct production decrease by around four orders of magnitude for asym, HOP, PL, χ QM and LCQM, and five orders of magnitude for HOL and AdS/CFT. Also, the HT contributions from semi-direct production decrease by about six orders of magnitude for all DAs. For example, for HOL, HT contributions decreases from 1.67×10^{-13} to 4.98×10^{-18} mb/GeV⁴ in direct production and 2.88×10^{-14} to 4.23×10^{-20} mb/GeV⁴ in semi-direct production. However, it should be emphasized that the difference between HT contributions from direct and semi-direct productions increase with increments of the transverse momentum p_T .

Moreover, with a view to make easy precise comparisons with the experimental results, we list individual HT contributions from direct and semi-direct hard-scattering processes at $p_T = 5$ GeV/c for each DAs in Table III. It is seen from this table that direct production HT contributions are dominated by the process $gg \rightarrow K^+K^-$ as expected. Semi-direct production HT contributions are dominated by the process $(\bar{q})g \rightarrow K^\pm(\bar{q})'$.

We exhibit the dependence of the HT, LT contributions, ratio of HT to LT and sum contribution on the rapidity $y = y_1 = y_2$ of kaon pairs varied in the range from -3 to 3 at $\sqrt{s} = 500$ GeV for each DA in Fig. 9. The rapidity distribution demonstrates the same dominant contributions in view of DAs as the ones in the

transverse momentum dependence of the cross section. It is seen that the HT and LT cross sections for all DAs of kaons except AdS/CFT, have a maximum at the point $y=0$. Additionally, they are almost symmetric according to $y=0$. However, the HT contributions in the region of positif rapidity are always somewhat larger than those in region of negative rapidity. When the rapidity goes up from 0 to 3, the HT cross sections decrease by around %70 for asym, HOP, PL, χ QM, LCQM and HOL, while grows by a factor of 1.5 for AdS/CFT. The LT contribution also decreases by %75. The ratio of HT to LT contributions is getting bigger slowly when y goes up from -3 to -2 and remains almost stable in a interval of rapidity from -2 to 2 and then continues to increase slowly with increments of rapidity from 2 to 3 for all DAs of kaons except AdS/CFT.

For different center of mass energies, the HT and LT differential cross sections are constructed and compared to a scaling with the variable $x_T = 2p_T/\sqrt{s}$. We have performed the above numerical results at $\sqrt{s} = 500$ GeV. To compared with other energies we also show the dependence of HT, LT contributions and ratio of HT to LT on the variable x_T ranging from 10^{-2} to 10^0 at the $p_T = 5$ GeV/c with rapidities of kaons $y = y_1 = y_2 = 0$ for momentum cut-off parameter $\Delta p = 0.5$ GeV/c in Figs. 10(a)-(b). These plots reveal that the distribution of variable x_T also demonstrates the same dominant contributions in view of DAs as the ones in the transverse momentum dependence of the cross section. Both HT and LT contributions increase slowly when x_T goes up from 0.01 to 0.2 and then decrease rapidly with increments of x_T from 0.2 to 1 for all DAs of kaons. Note that the decrease in the contributions is fast since the x_T is in the vicinity of 1, namely, $\sqrt{s} \sim 2p_T$. The ratio of HT to LT contributions remain almost stable in a large

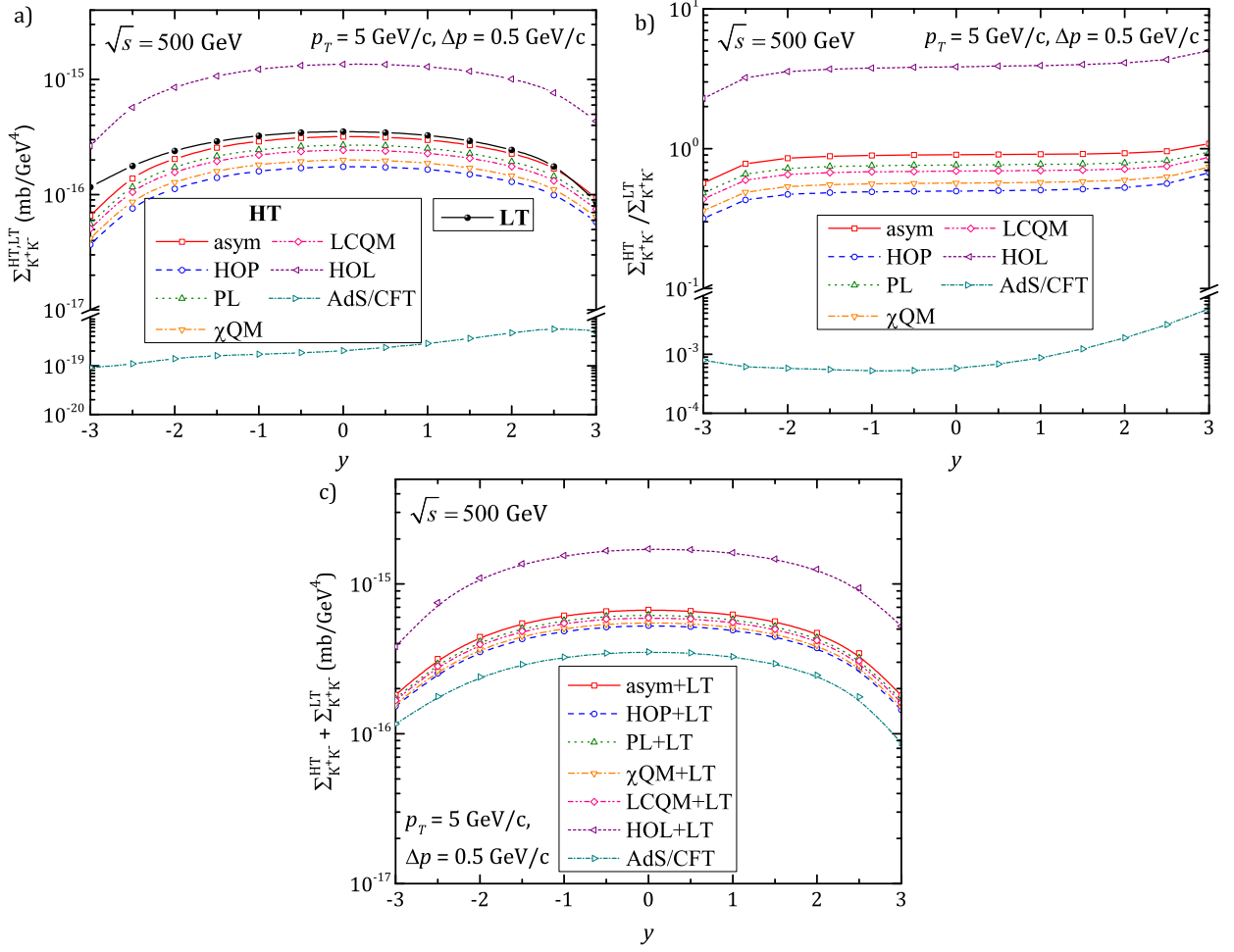


FIG. 9. a) LT and HT contributions to charged-kaon pair production $p\bar{p} \rightarrow K^+K^-X$, b) ratio of HT to LT and c) sum of these contributions as a function of the rapidity $y = y_1 = y_2$ of kaon pairs for momentum cut-off parameter $\Delta p = 0.5$ GeV/c and $p_T = 5$ GeV/c at $\sqrt{s} = 500$ GeV.

interval of x_T . This means that the ratio is less sensitive according to varying the center-of-mass energy.

V. SUMMARY AND PROSPECTS

In this work, the HT contributions, which are included the direct and semi-direct productions of the hard scattering process, to large- p_T kaon pair production in $p\bar{p}$ collisions have been discussed and the dependence of HT contributions on kaon-DAs predicted by light-cone formalism, the light-front quark model, the nonlocal chiral quark model and the light-front holographic AdS/CFT approach have been addressed.

It is observed that the results are significantly depend on the DAs of kaon, and can, hence, be used for their research. The basic size of the HT cross sections is seen to differ by several orders of magnitude depending on the choice of DAs of the produced kaons. The DAs of

LCQM, HOP, PL, and χ QM give results which are close in shape to those for the asymptotic DA, whereas HT contributions for HOL are larger than them by one order of magnitude and for AdS/CFT are smaller by three orders of magnitude.

The ratio of HT to LT contributions allows us to determine such regions in the phase space where HT contributions are essentially observable. This ratio is sensitive to the transverse momentum p_T and the momentum cut-off parameter Δp which is the detection limit for accompanying particles. For a small value of Δp and a large value of p_T , HT contributions yield considerably larger values. While the HT effect on cross section is small at the low p_T region, its effect becomes significant at the large p_T region compared to the LT contribution.

It is obvious that total contribution of direct production hard-scattering processes is larger than ones of semi-direct production processes in most cases. The HT process $gg \rightarrow K^+K^-$ gives the largest contribution to the inclusive cross section at large p_T for all DAs. How-

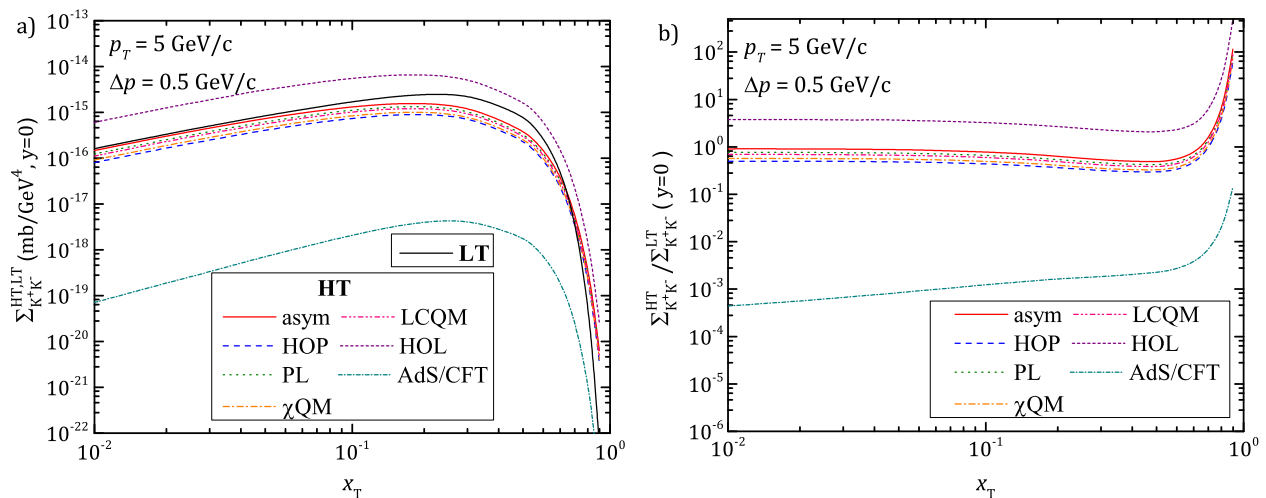


FIG. 10. a) LT and HT contributions to charged-kaon pair production $p\bar{p} \rightarrow K^+K^-X$ and b) ratio of HT to LT contributions as a function of the variable x_T for momentum cut-off parameter $\Delta p = 0.5$ GeV/c at $p_T = 5$ GeV/c.

ever, among semi-direct production processes, the process $qg \rightarrow K^\pm q'$ or $\bar{q}g \rightarrow K^\pm \bar{q}'$ has dominant contributions for all DAs.

The rapidity distribution exhibits the same dominant contributions in view of DAs as the ones in the transverse momentum dependence of the cross section. The HT contributions are enhanced in the region of positive rapidity.

Consequently, we can point out that the HT processes for large- p_T kaon pair production have a non-negligible contribution, where the kaons are produced directly in the hard-scattering subprocess, rather than by gluon and quark fragmentation. Inclusive kaon pair production provides a significant test case in which HT contributions dominate those of LT in certain kinematic regions. The HT contributions can be used to theoretical interpreta-

tion of the future experimental data for the charged kaon pair production in $p\bar{p}$ collisions. The results of this work will be helpful to providing a basic test of the short distance structure of QCD as well as to determine more precise DAs of kaon.

ACKNOWLEDGMENTS

M. Demirci is grateful to T. M. Aliev for useful discussions. A. I. Ahmadov is grateful for the financial support by the Science Development Foundation under the President of the Republic of Azerbaijan-Grant no: EIF/MQM/Elm-Tehsil-1-2016-1(26)-71/11/1. We have drawn the corresponding Feynman diagrams with the help of the program JaxoDraw [51].

-
- [1] J. F. Owens, *Rev. Modern Phys.* **59**, 465 (1987).
[2] F. Arleo, S. J. Brodsky, D. S. Hwang, and A. M. Sickles, *Phys. Rev. Lett.* **105**, 062002 (2010).
[3] V. N. Baier and A. Grozin, *Phys. Lett. B* **96**, 181 (1980).
[4] E. L. Berger, T. Gottschalk, and D. Sivers, *Phys. Rev. D* **23**, 99 (1981).
[5] J. A. Bagger and J. F. Gunion, *Phys. Rev. D* **25**, 2287 (1982).
[6] J. A. Bagger and J. F. Gunion, *Phys. Rev. D* **29**, 40 (1984).
[7] A. I. Ahmadov, C. Aydin, and O. Uzun, *Phys. Rev. D* **89**, 014018 (2014), and references therein.
[8] E. Pohjoisaho, *J. Phys. Conf. Ser.* **589**, 012016 (2015).
[9] S. J. Brodsky and A. Sickles, *Phys. Lett. B* **668**, 111 (2008).
[10] G. Curci, M. Greco, and Y. Srivastava, *Nucl. Phys. B* **159**, 451 (1979).
[11] G. Curci, M. Greco, and Y. Srivastava, *Phys. Rev. Lett.* **43**, 834 (1979).
[12] C. Berger *et al.* (PLUTO Collaboration), *Phys. Lett. B* **100**, 351 (1981).
[13] Y. I. Dokshitzer, G. Marchesini, and B. R. Webber, *Nucl. Phys. B* **469**, 93 (1996).
[14] M. Ciafaloni, D. Colferai, G. P. Salam, A. M. Stasto, *Phys. Rev. D* **66**, 054014 (2002).
[15] A. V. Kotikov, A. V. Lipatov, N. P. Zotov, *J. Exp. Theor. Phys.* **101**, 811 (2005).
[16] B. I. Ermolaev, M. Greco, and S. I. Troyan, *Eur. Phys. J. Plus* **128**, 34 (2013).
[17] C. D. Roberts and A. G. Williams, *Prog. Part. Nucl. Phys.* **33**, 477 (1994).
[18] J. M. Cornwall, *Phys. Rev. D* **26**, 1453 (1982).
[19] L. von Smekal, A. Hauck, and R. Alkofer, *Ann. Phys.* **267**, 1 (1998).
[20] R. Alkofer and L. von Smekal, *Phys. Rep.* **353**, 281 (2001).

- [21] F. Abe *et al.*, *Phys. Rev. Lett.* **61**, 1819 (1988).
- [22] D. E. Acosta *et al.*, *Phys. Rev. D* **65**, 072005 (2002).
- [23] T. Aaltonen *et al.* (CDF Collaboration) *Phys. Rev. D* **79**, 112005 (2009); **82**, 119903 (E) (2010).
- [24] C. Albajar *et al.* (UA1 Collaboration), *Nucl. Phys. B* **335**, 261 (1990).
- [25] K. Djagouri, J. J. Dugne, C. Carimalo and P. Kessler, *Z. Phys. C* **45**, 267 (1989).
- [26] C. R. Ji, and F. Amiri, *Phys. Rev. D* **42**, 3764 (1990).
- [27] L. A. Harland-Lang, V. A. Khoze, M. G. Ryskin and W. J. Stirling, *Eur. Phys. J. C* **71**, 1714 (2011).
- [28] Y. Wang, Y. M. Bystritskiy and E. Tomasi-Gustafsson, *Phys. Rev. C* **95**, 045202 (2017).
- [29] R. Baier, J. Engels, and B. Petersson, *Z. Phys. C-Particles and Fields* **2**, 265 (1979).
- [30] G. P. Lepage and S. J. Brodsky, *Phys. Rev. D* **22**, 2157 (1980).
- [31] J. F. Gunion and B. Petersson, *Phys. Rev. D* **22**, 629 (1980).
- [32] J. Binnewies, B. A. Kniehl, G. Kramer, *Z. Phys. C* **65**, 471 (1995).
- [33] A. D. Martin, W. J. Stirling, R. S. Thorne, and G. Watt, *Eur. Phys. J. C* **63**, 189 (2009).
- [34] A. I. Ahmadov and M. Demirci, *Int. J. Mod. Phys. A* **28**, 1350077 (2013).
- [35] A. I. Ahmadov and M. Demirci, *Phys. Rev. D* **88**, 015017 (2013).
- [36] M. Demirci and A. I. Ahmadov, *Phys. Rev. D* **89**, 075015 (2014).
- [37] S. D. Ellis, M. Jacob, and P. V. Landshoff, *Nucl. Phys. B* **108**, 93 (1976).
- [38] S. J. Brodsky, T. Huang, and G. P. Lepage, *Particles and Fields 2* (Springer, Boston, MA 1983), pp 143-199.
- [39] V. L. Chernyak, A. R. Zhitnitsky and I. R. Zhitnitsky, *Nucl. Phys. B* **204**, 477 (1982); Erratum: [*Nucl. Phys. B* **214**, 547 (1983)].
- [40] V. L. Chernyak, A. R. Zhitnitsky and I. R. Zhitnitsky, *Sov. J. Nucl. Phys.* **38**, 775 (1983).
- [41] V. L. Chernyak and A. R. Zhitnitsky, *Phys. Rept.* **112**, 173 (1984).
- [42] G. P. Lepage and S. J. Brodsky, *Phys. Lett. B* **87**, 359 (1979).
- [43] C. R. Ji, P. L. Chung and S. R. Cotanch, *Phys. Rev. D* **45**, 4214 (1992).
- [44] H. M. Choi, and C. R. Ji, *Phys. Rev. D* **95**, 056002 (2017).
- [45] S. I. Nam and H. C. Kim, *Phys. Rev. D* **74**, 096007 (2006).
- [46] A. V. Efremov and A. V. Radyushkin, *Theor. Math. Phys.* **42**, 97 (1980).
- [47] S. J. Brodsky and G. F. de T eramond, *Phys. Rev. Lett.* **96**, 201601 (2006).
- [48] A. Vega, I. Schmidt, T. Branz, T. Gutsche, and V. E. Lyubovitskij, *Phys. Rev. D* **80**, 055014 (2009).
- [49] S. J. Brodsky, G. P. Lepage, and P. B. Mackenzie, *Phys. Rev. D* **28**, 228 (1983).
- [50] T. Buran *et al.*, *Nucl. Phys. B* **116**, 51 (1976).
- [51] D. Binosi and L. Theussl, *Comput. Phys. Commun.* **161**, 76 (2004).